

Plasma enhanced atomic layer etching of high-k layers on WS₂

Special Collection: [Atomic Layer Etching \(ALE\)](#)

J.-F. de Marneffe ; D. Marinov; A. Goodyear; ... et. al



Journal of Vacuum Science & Technology A 40, 042602 (2022)

<https://doi.org/10.1116/6.0001726>



View
Online



Export
Citation

CrossMark

Related Content

First-principles study of graphene adsorbed on WS₂ monolayer

Journal of Applied Physics (November 2013)

Thermoelectric properties of WS₂ monolayer

AIP Conference Proceedings (October 2020)

Preparation of alternating MoS₂ and WS₂ single layers to form a new MoWS₄ structure

Journal of Applied Physics (February 1990)



Instruments for Advanced Science

- Knowledge
- Experience
- Expertise

Click to view our product catalogue

Contact Hiden Analytical for further details:
www.HidenAnalytical.com
info@hiden.co.uk

Gas Analysis



- dynamic measurement of reaction gas streams
- catalysis and thermal analysis
- molecular beam studies
- dissolved species probes
- fermentation, environmental and ecological studies

Surface Science



- UHV TPD
- SIMS
- end point detection in ion beam etch
- elemental imaging - surface mapping

Plasma Diagnostics



- plasma source characterization
- etch and deposition process reaction kinetic studies
- analysis of neutral and radical species

Vacuum Analysis



- partial pressure measurement and control of process gases
- reactive sputter process control
- vacuum diagnostics
- vacuum coating process monitoring

Plasma enhanced atomic layer etching of high-k layers on WS₂

Cite as: J. Vac. Sci. Technol. A 40, 042602 (2022); doi: 10.1116/6.0001726

Submitted: 29 December 2021 · Accepted: 29 April 2022 ·

Published Online: 26 May 2022



J.-F. de Marneffe,^{1,a)}  D. Marinov,¹  A. Goodyear,²  P.-J. Wyndaele,^{1,3}  N. St. J. Braithwaite,⁴  S. Kundu,¹ 
I. Asselberghs,¹ M. Cooke,² and S. De Gendt^{1,3} 

AFFILIATIONS

¹imec v.z.w., Kapeldreef 75, B-3001 Leuven, Belgium

²Oxford Instruments Plasma Technology, Yatton, Bristol BS49 4AP, United Kingdom

³Department of Chemistry, KU Leuven, Celestijnenlaan 200F, 3001 Leuven, Belgium

⁴Department of Physical Sciences, The Open University, Milton Keynes MK7 6AA, United Kingdom

Note: This paper is part of the 2023 Special Topic Collection on Atomic Layer Etching (ALE).

a) Author to whom correspondence should be addressed: marneffe@imec.be

ABSTRACT

The etching of HfO₂ and ZrO₂ high-k dielectrics is studied using plasma enhanced atomic layer etching. The etching method relies on a continuous argon inductively coupled plasma discharge in which reactive gases are pulsed, followed by substrate biasing; both steps are separated by purge periods. It is found that pure BCl₃ is too chemically active while a Cl₂-BCl₃ allows a high process synergy; in addition, the latter gives a high selectivity to SiO₂. The optimal etch conditions are applied to high-k layers deposited on top of WS₂ transition metal dichalcogenide. Postetch analysis shows negligible tungsten and sulfur depletion as well as negligible change in optical (Raman) response of the 2D layer, indicating that atomic layer etching concepts allows us to prevent WS₂ material loss or damage.

Published under an exclusive license by the AVS. <https://doi.org/10.1116/6.0001726>

I. INTRODUCTION

Two-dimensional transition metal dichalcogenides (2D-TMDCs), such as WS₂, are considered as alternative channel materials for future CMOS logic technology due to their reduced short channel effect compared to bulk silicon.^{1–4} Compared to MoS₂, WS₂ shows higher bandgap,⁵ larger carrier mobility,⁶ and ambipolar characteristic,^{5,7} enabling NMOS and PMOS operation under a common gate stack. Exceptional properties of TMDCs were demonstrated on exfoliated flakes, typically using large device dimensions and non-scalable fabrication techniques. On the contrary, large-scale integration of these materials into sophisticated nanoscale devices is challenging.^{8,9} The insertion of 2D TMDCs into very large-scale integration (VLSI) manufacturing requires to comply as much as possible to processing methods and device geometries established for Si CMOS. Wafer-scale fabrication requirements involve technological steps such as growth, deposition, transfer, cleaning (using organic or water-based solutions), doping, polishing, and etching, which are all presumed harmful toward highly sensitive and fragile 2D monolayer crystals.

In terms of materials, significant progress has been made in recent years on synthetic 2D-TMDC materials, using wafer-scale growth methods such as metal-organic chemical vapor deposition (MOCVD)^{10–13} and plasma enhanced atomic layer deposition (PEALD).^{14–17} For building VLSI compliant transistor devices, channel gating preferably relies on wide bandgap oxide dielectrics with EOT below 1 nm, known for their low defectivity, low leakage, and high permittivity. The growth of high quality high-k dielectrics in the nanometer range has been enabled by atomic layer deposition (ALD), which require a functionalized surface for nucleation. As a consequence, the low-damage growth of uniform, closed high-k oxide films is particularly challenging on chalcogen-terminated TMDCs because of the lack of available sites for chemisorption of ALD precursors on the 2D crystal surface. Precursor attachment by physisorption, which has a much lower bonding energy than chemisorption,^{18,19} has been explored. Also, approaches are being investigated to facilitate chemisorption, going from low-damage TMDC surface activation,²⁰ use of molecular seeding layers (covalent or noncovalent functionalization, see Ref. 21), Van der Waals bonded

hydrophilized 2D buffer layers,²² and sputter deposition of (oxidized) metals. Recent progress relies on TMDC surface saturation by high-pressure precursor vapors (TMA soak method).²³ Cleaning using liquid solutions is another challenging aspect of 2D-TMDC processing, mainly caused by 2D delamination due to water/solvent intercalation at the 2D–substrate interface. Dry cleaning using plasma processes has recently been investigated for PMMA residues on WS₂,²⁴ demonstrating high cleaning capability with low 2D damage.

Contacts to 2D materials are the subject of intense research and controversy on the nature of materials and interfaces,^{25–27} stacking of contact layers, deposition method,²⁸ and doping technique.^{25,29,30} Large-scale full wafer fabrication methods require electrical contacts to be preferentially built via a subtractive approach where, after a sacrificial mask is lithographically printed on the structure, the predeposited dielectric is etched away, exposing the channel, and then filled with the appropriate metal. In order to minimize device footprint (maximize packing density), the dielectric etching must be anisotropic (etching along the vertical direction). With the additional requirement to be selective to the 2D channel material, the preferred technique for contact patterning is plasma etching, which is currently an industrial standard thanks to its versatility and high throughput capability.

Recent works devoted to the study of TMDCs exposed to plasma were focusing on layer-by-layer etching of MoS₂, using either Ar plasma etching,³¹ CF₄ etching,³² Ar–Cl₂ atomic layer etching,¹⁸ or SF₆–N₂.³³ All these studies indicate that MoS₂ can be etched rather easily by fluor- and chlorine-based plasmas; this conclusion can be extended to WS₂. Regarding the plasma-based removal of layers selective to TMDCs, essentially two studies were published, the first focusing on the selective etching of Si on WS₂, using Ar/Cl₂ plasma atomic layer etching,³⁴ and the second on PMMA dry cleaning using H₂ downstream plasma.²⁴ The plasma chemistries studied in the above papers, based on Cl₂ and SF₆, are typically nonpassivating, and, therefore, intrinsically less selective. Finally, previous experience in edge contact fabrication showed that high bias continuous wave (CW) BCl₃ plasma is not selective to MoS₂ or WS₂.⁹ As shown above, the etch challenges brought by 2D materials require to study alternative plasma approaches, enabling softer material removal, i.e., less damaging to the sensitive TMDC layers. Recently, two major technological improvements of plasmas were studied. First, pulsing the plasma source (and/or bias) on the millisecond scale³⁵ to reduce the ion velocity distribution function to lower energies. Second, moving into a atomic layer etching (ALE)³⁶ mode, where surface activation and layer removal are taking place in time-separated steps, also aiming at reducing surface bombardment during the removal step.

In the present paper, we investigate the use of plasma enhanced atomic layer etching (PE-ALE) for the selective and low-damage removal of two mainstream high-k dielectric oxides, HfO₂ and ZrO₂ [both with dielectric constant $k \sim 25$ (Ref. 37)]. After describing the experimental details, the first part of the study covers the optimization of the PE-ALE process, aiming at maximum ALE synergy, finite etch rate, smooth postetch surface morphology, and selectivity toward PECVD SiO₂. This last requirement is motivated by two reasons: first, SiO₂ is the usual premetal dielectric deposited on top of the thin high-k film and second,

SiO₂ is used as a masking layer. The second part of the study describes the application of the optimized PE-ALE processes to WS₂ films passivated with HfO₂ and ZrO₂ dielectrics.

II. EXPERIMENTAL DETAILS

A. Materials

WS₂ films were deposited by plasma enhanced atomic layer deposition (PEALD) from WF₆, H₂S, and H₂ plasma in a hot-wall, showerhead-type PECVD reactor with direct (RF) plasma capability, connected to an Eagle12TM platform from ASM. Substrates used for the growth were 300 mm silicon wafers, coated with 85 nm of PECVD SiO₂. The PEALD reaction cycle consists of three reactions: a WF₆ reaction, a H₂ plasma reaction, and a H₂S reaction at a pressure of 2 Torr. Further details on the PEALD growth method can be obtained in Refs. 14–16.

After WS₂ deposition, a Si nucleation seed layer was deposited by means of magnetron sputtering, in a Canon-Anelva C-7100GT 5-PVD system, with zero bias voltage applied to the wafer. Three splits were used, with nominal thicknesses of 0.4, 0.7 and 1.0 nm. In this range of thicknesses, the deposited Si films were not closed.

Thin HfO₂ and ZrO₂ films (6 nm) are obtained by performing Atomic Layer Deposition (ALD) in a 300 mm, top-flow ALD reactor from Applied Materials. Tetrakis(EthylMethylAmino) Hafnium (TEMAH) and Tetrakis(EthylMethylAmino) Zirconium (TEMAZ) are used as the Hf and Zr precursor, respectively, while water is applied as the oxidizer. Both HfO₂ and ZrO₂ are deposited at a reactor temperature of 250 °C. This leads to the formation of continuous high-k films. The quality and electrical characteristics of the obtained high-k layer is described in details in the paper by Huyghebaert *et al.*¹

SiO₂ wafers used in this work were deposited by PECVD using a PlasmaPro 800 PECVD from Oxford Instruments Plasma Technology.

B. Plasma processes

The films were etched in a PlasmaPro 100 Cobra chamber with a 300 mm ICP source, from Oxford Instruments Plasma Technology. The plasma chamber is equipped with the atomic layer etching (ALE) kit. The ALE plasma conditions used in this work are based on a continuous Ar discharge (500 W ICP source, 100 SCCM Ar) at a fixed pressure of 10 mT. The ICP discharge is maintained all along the ALE cycles. The cycles are consisting of two main steps, separated by 6 s purges: a short pulse (few tens of milliseconds, without bias) during which reactive gases are injected in the plasma (BCl₃ or Cl₂/BCl₃), followed by a biased step with only Ar, of a few seconds (see Fig. 1). The wafer table was maintained at 0 °C. The samples, originally 300 mm wafers, were cut into smaller coupons that were pasted using Fomblin® oil on Al₂O₃-coated Si carrier wafers. It was found that the ALE process is very sensitive to fluorine contamination released by Fomblin® oil residues on the carrier wafer.

To estimate the bias power impact in the Ar plasma activation step, the ion velocity distribution functions were measured by a retarding field analyzer (RFEA), which was placed into the chamber. This system (Semion sensor by Impedans) consists of an

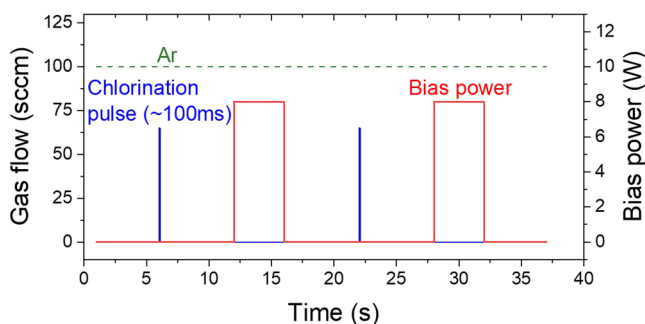


FIG. 1. Schematic representation of gas flows and applied bias power during the PE-ALE process sequence used in this work. See the text for more details.

orifice and an additional grounded grid confining the ion influx. A second grid behind this orifice allows us to discriminate the ion energies (by applying a retarding voltage), and a collector measures the incoming ion flux (collector current). The ion velocity distribution function (IVDF) is proportional to the derivative of the collector current with respect to the retarding voltage.³⁸ The IVDF characteristics, related to the current work, were published in a previous paper.³⁴

C. Characterization methods

Pre- and postetch metrology relied on spectroscopic ellipsometry (SE), atomic force microscopy (AFM), Raman spectroscopy, x-ray photoelectron spectroscopy (XPS), and Rutherford backscattering (RBS). SE was performed using a Woollam M-2000 ellipsometer and a Cauchy model. Atomic force microscopy (AFM) images were acquired in tapping mode in ambient using a Bruker Nanoscope V/ICON PT using an OCML-AC160TS tip. The Raman spectroscopy measurements were performed using a Horiba Jobin-Yvon HR800 instrument with a 532 nm laser excitation. The excitation beam was focused on the WS₂ surface using a 100× objective with a spot size of 1 μm. Raman measurements were performed at room temperature in ambient environment. Chemical analysis of the sample were done by x-ray photoelectron spectroscopy (XPS). The measurements were carried out in Angle Integrated mode using a Theta300 system from ThermoInstruments. A monochromatized Al Kα x-ray source (1486.6 eV) was used with a spot size of 400 μm. The energy calibrations were made against the C1s peak to compensate for charging effects during analysis. The film composition is characterized by Rutherford backscattering spectroscopy (RBS) to quantify the areal density of metals (Zr, Hf, W) and S, and hence the composition (i.e., S/W ratio), using a 1.52 MeV He⁺ ion beam and 25 nA beam current. The incident ion beam impinges at 11° with respect to the sample normal, and the detector is placed at a scattering angle of 170°.

III. RESULTS AND DISCUSSION

Atomic layer etching aims at disentangling surface activation from surface desorption of etch products by confining them in time-separated and self-limiting steps. Plasma ALE consist of two

steps: first a modification step, followed by a plasma activated removal step. In the modification step, the upper surface layer is chemically modified to lower its bonding energy to the bulk layer beneath. In the removal step, energy (heat, kinetic, chemical) is brought to the surface, allowing the release of volatile by-products; in a plasma-based ALE process, this step usually consist in physical bombardment by noble gas ions. Taking silicon as an example of an element to be etched, the step A consist in plasma chlorination of the surface to form easily desorbing SiCl_x species; followed by the step B where the SiCl_x layer is physically desorbed by a (biased) Ar plasma. Etching occurs by repeating this A–B–A–B– . . . cycling as many time as necessary to reach the target depth. The main difficulty with ALE is self-limitation, i.e., to tune the process in such a way that etching occurs only by the combined steps A and B, i.e., each stand-alone step (A or B) does not remove anything by itself. This requires, for step A, a careful selection of the reactants used for surface modification (halogens, O₂, . . .), as well as their dose on the surface, and for step B, a precise selection of the bombarding species (Ar, Xe, other), their energy and dose. The surface mechanisms occurring during plasma ALE are different from the usual continuous wave reactive ion etching (RIE), where, under simultaneous bombardment by energetic noble atoms and an inbound flux of reactive chemicals, the etched surface is brought into a steady-state configuration where adsorption, activation, diffusion, and desorption all occur at the same time. In this case, once steady state is reached (sometimes few seconds), all these processes occur in a so-called “RIE layer” which can be several nanometers thick. Atomic layer etching aims at reducing the thickness of this reaction layer to below 1 nm, ideally to the thickness of a crystalline lattice unit. Therefore, plasma ALE can be referred as an etch process which remains transient at all times since the RIE layer cannot reach steady state and is reset at each cycle.

A. Plasma enhanced atomic layer etch of HfO₂ and ZrO₂

The plasma etching of HfO₂ and ZrO₂, using continuous wave (CW) RIE, has been largely studied in the last two decades. Although several halogen-based mixtures were tried, the most successful etch method is based on Cl₂/BCl₃ and was best described, for HfO₂, in the papers by Martin *et al.*^{39,40} Essentially, the use of boron in the plasma chemistry creates energetically favorable reaction pathways leading to the formation of relatively volatile B_xO_yCl_z-containing etch products, facilitating the removal of oxygen from the surface. The boron-induced removal of oxygen enables the Hf to react with chlorine radicals and be removed by energetic ions; furthermore the heavier mass of B-containing ions increase their momentum at constant voltage bias, enhancing further the removal of HfO₂. It was also found that, in pure BCl₃ plasma, a deposition mechanism leading to the formation of a BCl_x-containing surface layer dominated at lower ion energies due to insufficient ion bombardment energy to remove nonvolatile boron-containing species in the RIE layer. Finally, the etch mechanisms of HfO₂ and ZrO₂ films using chlorine-based RIE plasma are rather identical due to similar volatility of ZrCl₄ (boiling point ~331 °C) and HfCl₄ (boiling point ~432 °C). The present work

starts from plasma conditions similar to those that were described in the papers by Martin *et al.*^{39,40}

The development of a plasma enhanced ALE process starts with the optimization of the dosing and sputter times, which need to be repeated each time the reactants and/or applied bias are modified. The dosing time corresponds to the time during which reactive chemicals (BCl_3 , Cl_2) are injected in the plasma, leading to optimal surface chlorination: if too low, the etch does not proceed due to lack of reactants, if too high, the etch might be hindered by the excessive coverage or deposition. The sputter time corresponds to the time necessary to remove part of or the whole chlorinated layer. For the optimal ALE process, using a bias power of 8 W (bias voltage of ~ 27 V) and a ratio $\text{Cl}_2/\text{BCl}_3 = 5.5$, it is found that an optimal dose time is in the range of 80–120 ms, while an optimal sputter time is around ~ 5 s, enabling high-k removal with limited SiO_2 recess.

Figure 2 shows the change in etch rate as a function of applied bias power during the Ar-sputter step (no bias is applied during the modification step). It compares three situations: without modification step (pure Ar sputtering), with pure BCl_3 and Cl_2/BCl_3 modification steps.

Concerning the pure sputtering case, the etch rate remain insignificant up to around ~ 10 W and then start to rise. The sputtering threshold E_{th} of both high-k dielectrics can be estimated using Steinbrüchel's formula,⁴¹

$$EY \sim \sqrt{E} - \sqrt{E_{th}}, \quad (1)$$

where EY is the etch yield (or etch rate), E is the energy of the ion impinging on the surface, and E_{th} is the threshold ion energy for etching. The energy of ions arriving at the surface (the DC bias) results from two contributions: DC bias = $(-V_{dc} + V_{pp})$. V_{dc} is the self-bias voltage arising from the RF bias applied to the wafer; it is directly measured during the etch experiment. The plasma potential V_{pp} for the used Ar discharge, was measured to be $V_{pp} \sim 11$ V, as determined by retarding field energy analyzer.³⁴ The sputtering threshold E_{th} is obtained by representing the etch rate as a function of $\sqrt{\text{DC bias}}$ and is calculated from the intersect of the $Y=0$ horizontal axis [Fig. 2(c)], giving the values $E_{th}(\text{HfO}_2) \sim 47$ eV and $E_{th}(\text{ZrO}_2) \sim 51$ eV. For HfO_2 , this value is slightly lower than what has been reported in the literature [~ 69 eV (Ref. 42)]. The main conclusion from these data is that, although the absolute etch yield is higher for HfO_2 than for ZrO_2 , both materials have a similar sputtering threshold.

Looking back at Figs. 2(a) and 2(b), it can be noted that similar trends are observed for HfO_2 [Fig. 2(a)] and ZrO_2 [Fig. 2(b)], as expected from their chloride by-product's boiling points and found in the literature. Compared to pure Ar sputtering, the introduction of a modification step has a significant impact, leading to a boost in removal rate and a shift of sputtering threshold toward lower values. This indicates that the presence of chlorine on the HfO_2 surface allows us to reduce the binding energy of surface atoms, which can then be sputtered away at a much lower energy. For Cl_2/BCl_3 , the extrapolated ALE threshold energy E_{thALE} is reduced to around 17 V (5 W) indicating that the formation of volatile by-products requires some finite energy input to proceed,

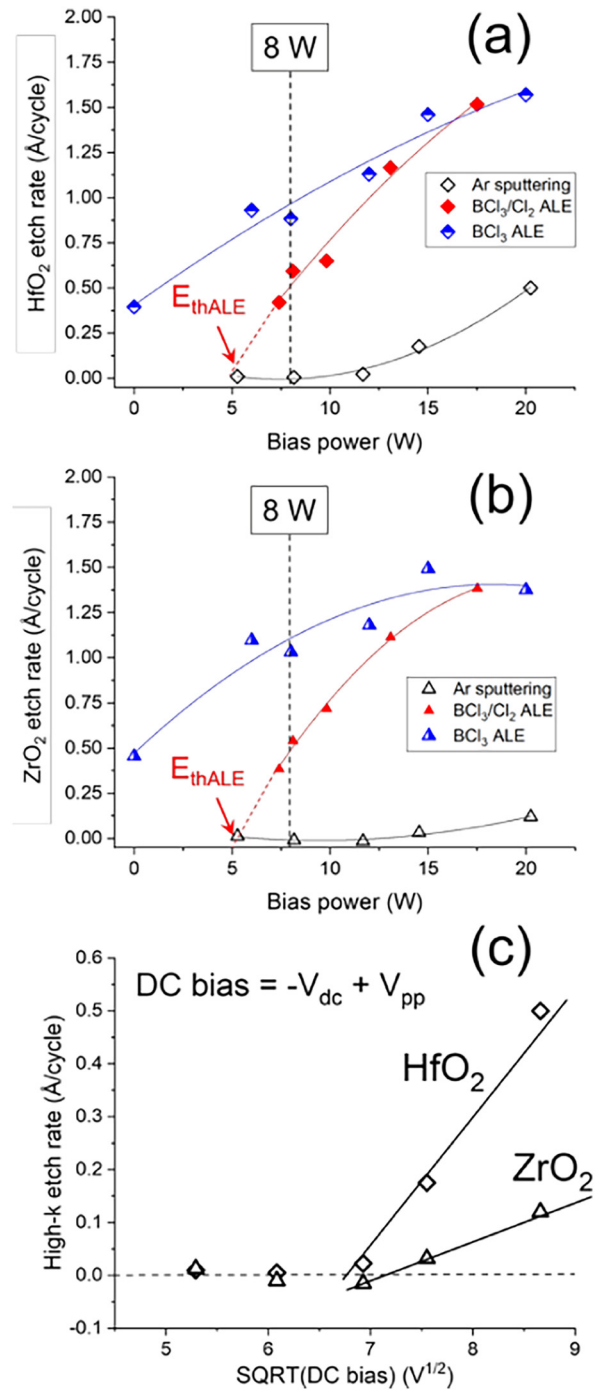


FIG. 2. Etch rate of HfO_2 (a) and ZrO_2 (b) for two different ALE etch processes and pure Ar plasma sputtering. Lines are polynomial fits serving as guides to the eye. Sputtering rates (c) for both high-k dielectrics as a function of $\sqrt{\text{DC bias}}$, allowing us to calculate the sputter threshold energy E_{th} . Note that for all experiments of figures (a) and (b), the applied bias power was reported, which need to be converted into self-bias voltage V_{dc} for building figure (c).

Downloaded from http://pubs.aip.org/avs/journal/article-pdf/doi/10.1116/6.0001726/16563782/042602_1_online.pdf

i.e., we are still in an ion-assisted etching mode. For pure BCl_3 , $E_{thALE} = 0$, as shown by the finite etch rate existing at 0 W bias (i.e., without Ar-sputter step). This means that the removal of surface atoms does not require much additional energy input coming from Ar ions, i.e., it is mostly chemically driven (~ 11 eV ions from the plasma voltage V_{pp} drop are enough to proceed to etch). Note that, even if non-negligible, the measured etch rate at 0 W bias, $\sim 0.4 \text{ \AA/cycle}$, when expressed in more classical etch rate units, is equivalent to a removal rate of 0.16 nm/min , i.e., one to two order of magnitude slower than what would be obtained in CW RIE.

More insight into the surface chemistry can be deduced from x-ray photoelectron spectroscopy, as shown in Fig. 3 for HfO_2 films. For the pure BCl_3 process, without applied bias, some B-Cl-O layer is formed, as indicated by the prominent B1s and Cl2p peaks that appear in the spectrum. The elemental composition indicates that this layer is boron-rich with a ratio B/Cl ~ 3 . Due to the significant contribution of the underlying HfO_2 layer in the XPS signal, the precise O content of the B-Cl(-O) layer is difficult to assess; however, the detected O amount surpass largely the level of Hf, indicating that some O is unambiguously bond to B and Cl, forming a boron-oxy-chloride layer. Furthermore, the presence of a significant Hf-O signal indicates that the B-Cl-O layer is rather thin, i.e., a few nanometers thick at maximum. This observation is different from what is observed in CW plasma made of pure BCl_3 , where BCl_x polymer deposition is observed without HfO_2 etching.^{40,43,44} In a CW plasma process, there is a constant flux of BCl_x species toward the film surface, while for our PE-ALE process, the flux of such species is timely constrained to the dose time, between 80 and 120 ms, while for the rest of the cycle no BCl_3 is injected in the chamber. During that period, the surface is

furthermore exposed to the Ar plasma, which even nonbiased, provided some low-energy surface bombardment. We can, therefore, assume that during the BCl_3 pulse, some BCl_x species deposit on the surface, from which a significant part does desorb afterward, reaching a steady-state (thin) B-Cl(-O) layer as shown in our XPS data. If some bias voltage is applied during the Ar-sputter step, the B and Cl contaminations are strongly reduced, indicating almost complete disappearance of the B-Cl(-O) layer, i.e., a nonhalogenated HfO_2 surface. For Cl_2/BCl_3 , with applied bias, the surface remains also free of B and Cl.

Using the above data, the following etch mechanisms can be postulated. First, the Cl_2 and Cl_2/BCl_3 pulses are essential to shift the sputtering threshold to lower energy, enabling some RIE-driven removal of the high-k layers. For pure BCl_3 , some finite etch rate is observed without Ar-sputter step together with the formation of a B-Cl(-O) layer on the surface. In this case, the high-k removal is essentially chemically driven and uses the B-Cl(-O) layer as a reservoir to form Hf-Cl-O_x and B-Cl-O_y volatile compounds that continuously desorb from the surface (including purge steps) since this layer is formed on the surface. When a (biased) Ar-sputter step is added, the B-Cl(-O) layer is removed cyclically, enhancing the HfO_x removal by RIE, i.e., leading to an higher etch rate. The case of the Cl_2/BCl_3 mixture offers a lower chemical reactivity with the surface since the threshold removal energy for ALE is extrapolated to $E_{thALE} \sim 17 \text{ V}$ (5 W) [see Figs. 2(a) and 2(b)], indicating that without Ar-sputter step, there will be no HfO_2 desorption occurring.

The ALE synergy, usually denoted by the symbol S , gives an estimate of the impact of the self-limited character of each of the modification and activation steps on the overall cyclic removal process. It is usually defined as⁴⁵

$$S(\%) = \frac{EPC - (\alpha + \beta)}{EPC} \times 100, \quad (2)$$

where EPC is the etch per cycle, α represents the amount of unintended etching in step A, and β represents the amount of sputtering of unmodified material in step B. The optimal process control occurs at maximum synergy, i.e., when both chemical etching in step A and sputter removal in step B are minimal. Referring to Figs. 2(a) and 2(b), it is clear that a high synergy cannot be met for pure BCl_3 since both high-k layers are removed even for 0 W applied bias power. Focusing exclusively on the Cl_2/BCl_3 mixture, the applied bias power need to be above 5 W ($>E_{thALE}$) but below $\sim 10 \text{ W}$ where material sputtering start to be effective. For our process, the optimal bias power is, therefore, set to 8 W. The comparison of ALE synergies for both BCl_3 and Cl_2/BCl_3 processes is summarized in Table I. Table I includes data for SiO_2 obtained for the Cl_2/BCl_3 mixture. Contrary to the high-k oxides, the SiO_2 shows a high sputter yield and no chemical etch with an EPC close to zero. Detailed ellipsometry measurements indicate the presence of a thick ($\sim 1 \text{ nm}$) B-Cl-O passivation layer deposited during the Cl_2/BCl_3 pulse, explaining this low EPC. The etching mechanism for SiO_2 does not obey the ALE rule and, therefore, synergy calculation is irrelevant for these particular conditions. Comparing the EPCs for HfO_2 , ZrO_2 , and SiO_2 , it appears that a high selectivity high-k: $\text{SiO}_2 \simeq 10$ is achieved for this specific process.

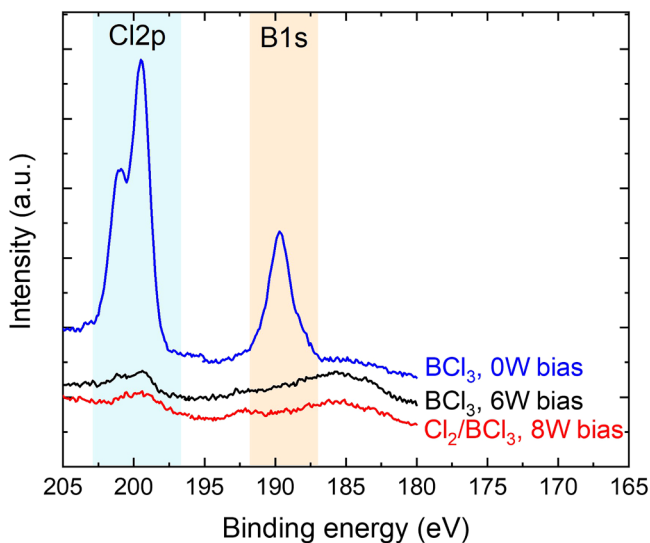


FIG. 3. X-ray photoelectron spectroscopy of the HfO_2 surface after exposure to various PE-ALE processes, focusing on the Cl2p (200 eV) and B1s (190 eV) bond energies.

Downloaded from http://pubs.aip.org/avs/jvst/article-pdf/doi/10.1116/6.0001726/16563782/042602_1_online.pdf

TABLE I. Etch rate data for each part of the PE-ALE processes investigated in this work, at fixed bias power of 8 W, allowing us to calculate the ALE synergy S [see Eq. (2)].

Material	8 W/5 s bias, 80 ms dose		Cl ₂ /BCl ₃		
	BCl ₃		Cl ₂ /BCl ₃		
	HfO ₂	ZrO ₂	HfO ₂	ZrO ₂	SiO ₂
Chemical etch/ α (Å)	0.41	0.47	0	0	0
Sputtering/ β (Å)	0	0	0	0	0.22
EPC (Å)	0.88	1.03	0.43	0.44	<0.04
ALE synergy/S	53%	54%	100%	100%	NA

The variations of process parameters have impact on the morphology of the HfO₂, as shown in Fig. 4, with a focus on dose time, Cl₂/BCl₃ ratio, and bias power. In optimal PE-ALE process conditions (sample B), the pristine HfO₂ roughness (sample A) does not change significantly. Increasing the dose time from 80 to 120 ms then 160 ms (samples B → D → F) leads to larger roughness, which can be attributed to B-Cl(-O) micromasking, as explained in the paper by Sungauer *et al.*⁴⁶ By increasing the dose, a thicker B-Cl(-O) layer is deposited on the HfO₂ surface, which cannot be fully removed by the subsequent Ar-sputter step, therefore preventing the etch of HfO₂ at the next cycle. A similar phenomenon occurs by

TABLE II. Process conditions used for the PE-ALE processes applied to the WS₂ passivated samples. The plasma pressure was set at 10 mT and ICP (source) power at 500 W.

PE-ALE type	Modification step			Ar-sputter step	
	Dosing time (ms)	BCl ₃ (SCCM)	Cl ₂ (SCCM)	Bias (W)	Time (s)
Cl ₂ /BCl ₃	80	10	55	8	5
BCl ₃	80	60	0	6	5

decreasing the Cl₂/BCl₃ ratio (samples B → C), therefore increasing the B/Cl ratio of the discharge and promoting the formation of a boron-rich B-Cl(-O) layer, which is known to condense easier at the surface.⁴⁰ Finally, the roughness increase caused by a longer dose can be compensated by a higher energy Ar-sputter step, which can remove efficiently the thicker B-Cl(-O) layer (samples D → E).

B. Removal of high-k oxide on WS₂

In this section, PE-ALE processes (see Table II) are applied to WS₂ samples passivated by high-k films. IMEC's WS₂

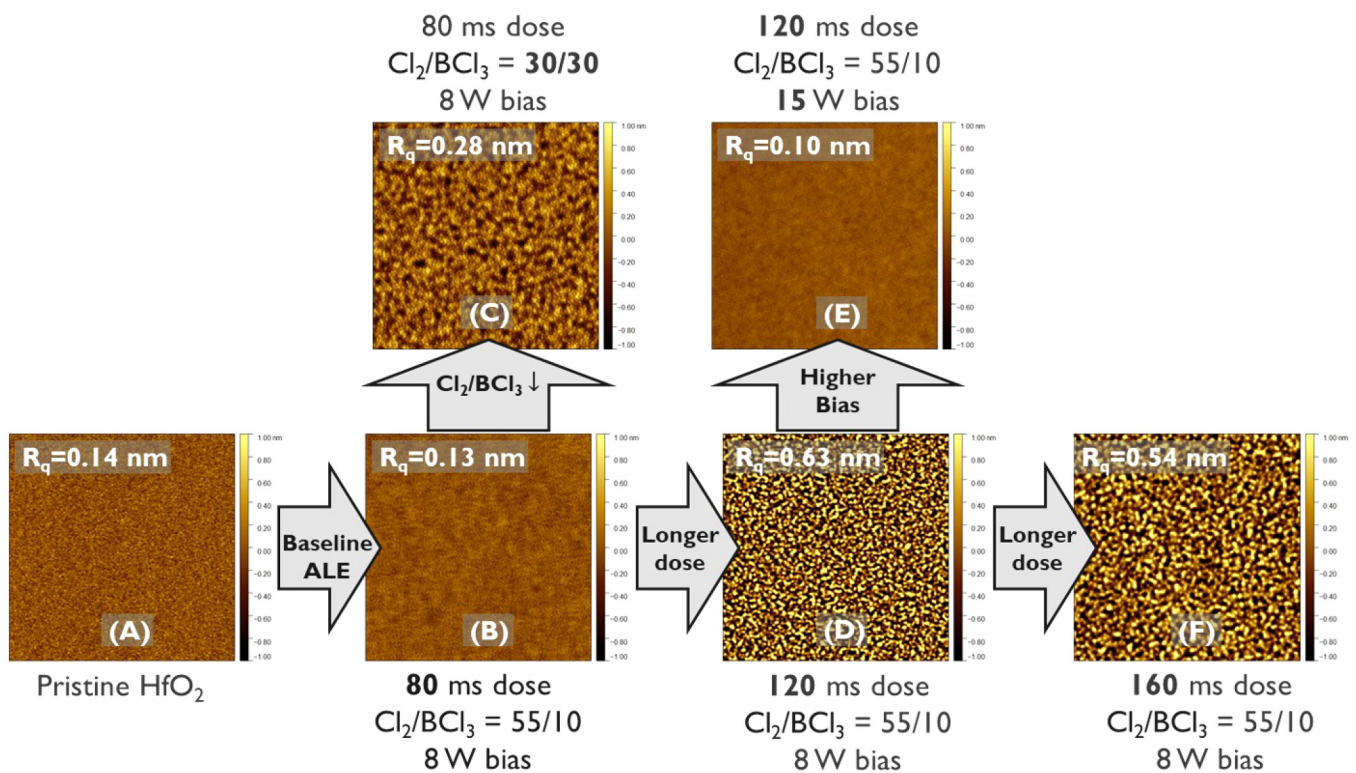


FIG. 4. Morphological evolution of the HfO₂ surface after being exposed to the optimal PE-ALE process and variations thereof, as measured by AFM. (a) Pristine HfO₂ surface; (b) after PE-ALE, optimal process conditions; (c) decreasing Cl₂/BCl₃ ratio; (d) longer dose time (80 → 120 ms); (e) higher bias during sputter step at dose time 120 ms; and (f) longer dose time (120 → 160 ms).

Downloaded from http://pubs.aip.org/avs/jvst/article-pdf/doi/10.1116/6.0001726/16563782/042602_1_online.pdf

process-of-record PEALD process was used to grow three monolayers thick WS₂ on 85 nm SiO₂. As WS₂ is intrinsically hydrophobic, the growth of dielectrics on top, using ALD, is challenging. In order to provide nucleation sites, Si was sputtered on the WS₂ surface by PVD for nominal thicknesses going from 0.4 to 1.0 nm; by subsequent ambient exposure, the Si oxidizes to form SiO₂ (hydrophilic). Those silicon oxide layers were not closed, even for the thicker one. Subsequently, 6 nm high-k layers were deposited by ALD. Further details can be found in Sec. II. The stack and goal are described in Fig. 5.

All samples were exposed to various number of cycles of either the BCl₃-only process (low synergy) or the mixed Cl₂/BCl₃ ALE process (high synergy, optimal), see conditions as detailed in Table II. Aiming at an over-etch of about ~10%, this amount to 50 cycles for the BCl₃-only process and 125 cycles for the Cl₂/BCl₃ process.

Figure 6 shows the elemental composition of the top surface for the pristine samples and after PE-ALE, as measured by Rutherford backscattering (RBS). Due to peak overlap, RBS cannot discriminate between the W and Hf signals. The first column on the left refers to the unpassivated sample, i.e., pristine WS₂, which is used as a reference to set the baseline W and S surface density. After high-k ALD, we can see a major increase in Zr density, by >10¹⁶ at/cm², corresponding to the formation of ZrO₂. A similar increase is observed for the convoluted Hf-W signal, corresponding to the formation of HfO₂. After PE-ALE, for both BCl₃-only and Cl₂/BCl₃ processes, the large Zr signal is quenched and fades within the RBS error bars; it must be noted that there is insignificant change in the W and S signal intensity, indicating that the WS₂ layer is essentially intact. A similar trend can be observed for the etch of HfO₂, despite the Hf-W convolution.

Figure 7 shows the optical response of the pristine samples and after PE-ALE, as measured by Raman spectroscopy. Figure 7(a) shows the main WS₂ Raman peaks for both high-k layers with a Si nucleation fixed at 0.7 nm (nominal thickness). For ZrO₂, the intensity and shape of the WS₂ peaks do not change significantly after PE-ALE etch, indicating little damage to the material. It must be highlighted that this is also the case with the pure BCl₃ process, which show a low ALE synergy (high chemical

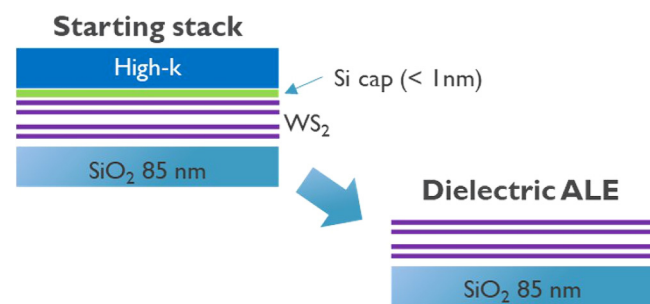


FIG. 5. Film stack used in this study. The PEALD WS₂ film is covered by a thin Si cap (nonclosed layer) which is used as a seed for subsequent ALD growth of 6 nm ZrO₂ or HfO₂. The high-k film is removed by PE-ALE, and the remaining WS₂ is evaluated then compared with the pristine film.

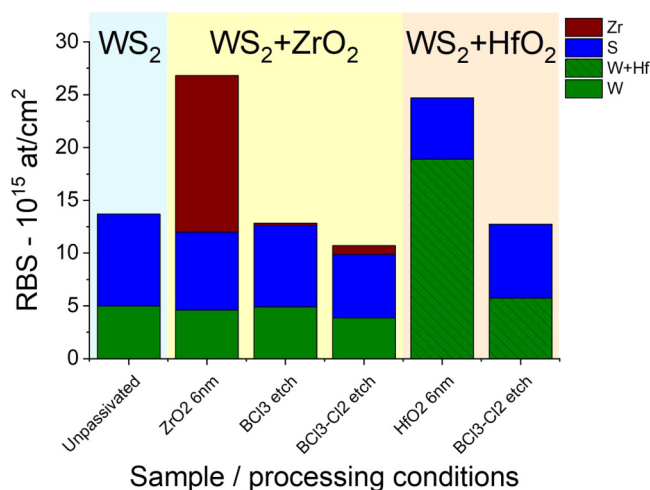


FIG. 6. Surface elemental composition as measured by Rutherford backscattering (RBS).

component). For the HfO₂, a small decrease in peak intensity is observed, indicating that the layer is slightly modified. Figure 7(b) shows the main WS₂ Raman peaks for ZrO₂, but with varying Si nucleation layer thicknesses, going from 0.4 to 1.0 nm nominal thicknesses (only one pristine sample is shown). As can be seen from the graph, after etch with the Cl₂-BCl₃ PE-ALE process, change is negligible indicating that the absence of WS₂ modification cannot be attributed to the presence of oxidized Si layer in-between WS₂ and ZrO₂.

Finally, some etch tests were performed on samples applying a higher number of cycles, going from 50 to 65 cycles for pure BCl₃ and 125 to 150 cycles for the Cl₂-BCl₃, corresponding to a significant over-etch of the WS₂ layer (corresponding to approximately ~30%–40% over-etch for both PE-ALE processes). For both conditions, applying such a large over-etch led to WS₂ damage.

We can conclude from these data that the PE-ALE processes studied in this work show limited WS₂ damage provided that the over-etch is kept to maximum ~10%; the level of damage is not linked to the thickness of the Si nucleation layer, which, knowing that none of these layer are closed, indicates that the low level of damage is a direct benefit of a reasonable HfO₂/ZrO₂-to-WS₂ selectivity for both PE-ALE studied processes. Both studied PE-ALE processes are rather different, as one is based on pure BCl₃ and the second one a Cl₂-BCl₃ mixture containing a large proportion of Cl₂ (~85%). As shown in the previous paragraph, the pure BCl₃ process has a significant chemical component, leading to a higher high-k etch rate (below ~10–12 W applied bias power). Despite this observation, it is observed that both processes show some selectivity toward WS₂. It is interesting to compare the present data to previously published work on MoS₂, in particular, to the papers by Heyne *et al.*³⁴ and Lin *et al.*⁴⁷ Although MoS₂ differs from WS₂, we can anticipate similar etch rates and mechanisms as the vapor pressures of the pure chlorides MoCl₅, WCl₅, and WCl₆ are very similar. Both papers study the effect of Ar/Cl₂

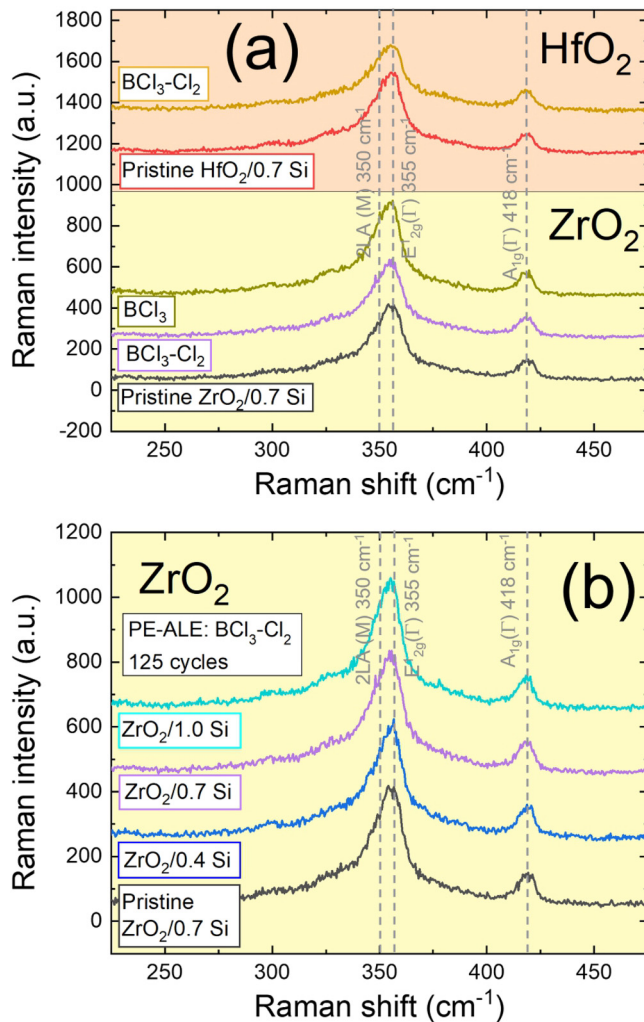


FIG. 7. Raman intensity for various samples, pristine and after high-k PE-ALE. (a) Varying PE-ALE processes and (b) varying Si nucleation layer at fixed number of PE-ALE cycles.

ALE on MoS₂, by means of Cl⁺ radical adsorption followed by Ar ion bombardment, and conclude that MoS₂ is etched at rates varying between 4 and 6.5 Å per cycle. The work by Heyne *et al.* is of high relevancy since it was performed in an identical tool as in the present study with similar baseline conditions (identical pressure, ICP source power, and flux of Ar) but higher DC bias voltage (33–45 V, as compared to 16–24 V/6–8 W in the present work). It was found that MoS₂ is etched at a rate of 3–4 Å/cycle, i.e., one order of magnitude higher than what is observed here. The mechanism was attributed to top surface desulfurization by the high energetic Ar-sputter step, leading to subsequent metal chlorination and removal. In the present work, the lower bias voltage used in the sputter step can bring the system below the sputtering threshold of the sulfur atoms composing the WS₂ top sulfur plane, leading to a

much slower W chlorination and removal. A second major difference with the process by Heyne *et al.* is the presence of BCl₃ as reactive gas or additive. By interaction with the top sulfur plane of WS₂, boron might form boron trisulfide (B₂S₃), a polymeric compound with high melting point (563 °C), acting as a passivant for underlying WS₂ protection. The presence of a silicon seed layer on WS₂, turning into SiO₂ upon ambient exposure (before ALD of the high-k layers), lead to Si-containing residues that cannot be precisely quantified with the methods used in the present paper (RBS will not discriminate Si seed residues from the SiO₂ substrate directly under the WS₂). Referring to Table I, those Si residues will not be removed by the Cl₂/BCl₃ PE-ALE process and a low over-etch percentage of only ~10%. If not removed by an alternative method, they will contribute to the capacitive equivalent thickness (CET) of the dielectric passivation, impacting negatively the electrical characteristics of the transistors (subthreshold swing slope, D_{it}). Residue removal methods, for instance, using wet cleaning with diluted HF need to be investigated as a complement to the PE-ALE presented in this paper.

IV. CONCLUSION

The present work studies the plasma enhanced atomic layer etch (PE-ALE) of high-k dielectrics (ZrO₂, HfO₂) selective to WS₂ transition metal dichalcogenide. The studied process relies on a cyclic method consisting of a continuous Ar plasma discharge in which halogen gas is pulsed followed by substrate biasing. Two halogen mixtures are considered, pure BCl₃ and Cl₂/BCl₃. The sputtering thresholds under Ar ion bombardment for HfO₂ and ZrO₂ are found to be similar with, respectively, 47 and 51 eV. By adding pulses of halogen gas, the sputtering threshold moves to lower energies and the high-k etch rates increase dramatically. By screening the bias power dependency of the etch process, it is found that pure BCl₃ process has a significant non-RIE (chemical) component, while the Cl₂/BCl₃ process is sputter-mediated, leading to ALE synergies of, respectively, 53%–54% and 100%. The plasma parameters of the Cl₂/BCl₃ discharge are optimized on the basis of the surface morphology change of HfO₂, leading, for the optimal conditions, to postetch AFM roughness similar to the pristine sample. Based on XPS analysis of the etched surfaces, it is deduced that, for the pure BCl₃ discharge, at low biasing the surface is coated by a boron-rich B–Cl(O) layer which act as a reservoir for forming volatile species all along the cycles. In the presence of Ar sputtering of high enough energy or in a diluted mixture (i.e., by addition of Cl₂), this reactive layer is quickly desorbed or does not form. In addition, it is found that the optimal PE-ALE conditions, using the Cl₂/BCl₃ process, show high selectivity to SiO₂, which is a clear asset when it is used as a masking material. The optimal BCl₃ and Cl₂/BCl₃ PE-ALE processes are then applied to a WS₂-(Si)-high-k stack. After removing the high-k layers, it is found that the WS₂ Raman peaks remain largely unchanged, indicating that the studied PE-ALE processes do develop some selectivity to the WS₂. It is suggested that the observed selectivity might be linked to a substrate biasing below the sputtering threshold of the sulfur atoms composing the layers and/or that a passivating B₂S₃ layer is formed on the surface.

ACKNOWLEDGMENTS

D. Marinov has received funding from the European Union's Horizon 2020 research and innovation program under Marie Skłodowska-Curie, Grant Agreement No. 752164. J.-F. de Marneffe received funding from the Graphene Flagship, Grant Agreement No. 952792. All authors acknowledge the support of imec's beyond CMOS program, imec's pilot line, and imec's materials and characterization (MCA) group. The authors thank Dr. Laura Nyns (imec) for the ALD of ZrO₂ and HfO₂ films and Dr. Benjamin Groven (imec) for the deposition of WS₂ films by PEALD.

AUTHOR DECLARATIONS

J.-F. de Marneffe (imec) coordinated the collaboration between imec v.z.w. and Oxford Instruments Plasma Technology (OIPT), performed data analysis, and drafted the manuscript; D. Marinov (imec) coordinated the technical aspects of the work, then executed the experimental part in collaboration with A. Goodyear (OIPT) and M. Cooke (OIPT). Both J.-F. de Marneffe and D. Marinov contributed equally to the study presented in this paper. P.-J. Wyndaele (imec/KULeuven) and S. Kundu (imec) participated in data interpretation and analysis. N. St. J. Braithwaite (Open University) provided the IVDF Semion system as well as support for IVDF measurement and data analysis. I. Asselberghs (imec) coordinates the 2D research activity at imec v.z.w. and enabled access to materials, wafers, and characterization. S. De Gendt (imec/KULeuven) coordinated the scientific activities led by D. Marinov and J.-F. de Marneffe. All co-authors agreed with the content of the manuscript.

Conflict of Interest

The authors have no conflicts to disclose.

DATA AVAILABILITY

The data that support the findings of this study are available from the corresponding author upon reasonable request.

REFERENCES

- C. Huyghebaert *et al.*, "2D materials: Roadmap to CMOS integration," in *2018 IEEE International Electron Devices Meeting (IEDM)* (IEEE, 2018), pp. 22.1.1–22.1.4.
- G. V. Resta, A. Leonhardt, Y. Balaji, S. De Gendt, P.-E. Gaillardon, and G. De Micheli, *IEEE Trans. Very Large Scale Integr. Syst.* **27**, 1486 (2019).
- D. Akinwande, C. Huyghebaert, C.-H. Wang, M. I. Serna, S. Goossens, L.-J. Li, H. S. P. Wong, and F. H. L. Koppens, *Nature* **573**, 507 (2019).
- Y. Liu, X. Duan, H.-J. Shin, S. Park, Y. Huang, and X. Duan, *Nature* **591**, 43 (2021).
- D. Braga, I. Gutiérrez Lezama, H. Berger, and A. F. Morpurgo, *Nano Lett.* **12**, 5218 (2012).
- W. Zhang, Z. Huang, W. Zhang, and Y. Li, *Nano Res.* **7**, 1731 (2014).
- G. Lee, S. Oh, J. Kim, and J. Kim, *ACS Appl. Mater. Interfaces* **12**, 23127 (2020).
- I. Asselberghs *et al.*, "Scaled transistors with 2D materials from the 300 mm fab," in *2020 IEEE Silicon Nanoelectronics Workshop (SNW)* (IEEE, 2020), pp. 67–68.
- I. Asselberghs *et al.*, "Wafer-scale integration of double gated WS₂-transistors in 300 mm Si CMOS fab," in *2020 IEEE International Electron Devices Meeting (IEDM)* (IEEE, 2020), pp. 40.2.1–40.2.4.
- H. Cun, M. Macha, H. Kim, K. Liu, Y. Zhao, T. LaGrange, A. Kis, and A. Radenovic, *Nano Res.* **12**, 2646 (2019).
- J. Mo, S. E. Kazzi, W. Mortelmans, A. N. Mehta, S. Sergeant, Q. Smets, I. Asselberghs, and C. Huyghebaert, *Nanotechnology* **31**, 125604 (2020).
- A. Cohen, A. Patsha, P. K. Mohapatra, M. Kazes, K. Ranganathan, L. Houben, D. Oron, and A. Ismach, *ACS Nano* **15**, 526 (2021).
- M. Chubarov *et al.*, *ACS Nano* **15**, 2532 (2021).
- B. Groven *et al.*, *Chem. Mater.* **29**, 2927 (2017).
- B. Groven *et al.*, *J. Vac. Sci. Technol. A* **36**, 01A105 (2018).
- B. Groven *et al.*, *Chem. Mater.* **30**, 7648 (2018).
- S. Balasubramanyam, M. J. M. Merkx, M. A. Verheijen, W. M. M. Kessels, A. J. M. Mackus, and A. A. Bol, *ACS Mater. Lett.* **2**, 511 (2020).
- K. S. Kim *et al.*, *ACS Appl. Mater. Interfaces* **9**, 11967 (2017).
- T. Park *et al.*, *RSC Adv.* **7**, 884 (2017).
- L. Cheng, X. Qin, A. T. Lucero, A. Azcatl, J. Huang, R. M. Wallace, K. Cho, and J. Kim, *ACS Appl. Mater. Interfaces* **6**, 11834 (2014).
- L. Daukiya, J. Seibel, and S. D. Feyter, *Adv. Phys. X* **4**, 1625723 (2019).
- P.-J. Wyndaele, J.-F. de Marneffe, and S. De Gendt, *ECS Meet. Abstr. MA2020-02*, 1348 (2020).
- X. Wu *et al.*, "Ald encapsulation of CVD WS₂ for stable and high-performance FET devices," in *2021 5th IEEE Electron Devices Technology Manufacturing Conference (EDTM)* (IEEE, 2021), pp. 1–3.
- D. Marinov *et al.*, *npj 2D Mater. Appl.* **5**, 17 (2021).
- Z. Gao, Z. Zhou, and D. Tománek, *ACS Nano* **13**, 5103 (2019).
- P.-C. Shen *et al.*, *Nature* **593**, 211 (2021).
- Y. Zheng, J. Gao, C. Han, and W. Chen, *Cell Rep. Phys. Sci.* **2**, 100298 (2021).
- Y. Liu *et al.*, *Nature* **557**, 696 (2018).
- H. Zhu, X. Gan, A. McCreary, R. Lv, Z. Lin, and M. Terrones, *Nano Today* **30**, 100829 (2020).
- Y. Wang, Y. Zheng, C. Han, and W. Chen, *Nano Res.* **14**, 1682 (2021).
- Y. Liu *et al.*, *ACS Nano* **7**, 4202 (2013).
- M. H. Jeon *et al.*, *Nanotechnology* **26**, 355706 (2015).
- S. Xiao, P. Xiao, X. Zhang, D. Yan, X. Gu, F. Qin, Z. Ni, Z. J. Han, and K. K. Ostrikov, *Sci. Rep.* **6**, 19945 (2016).
- M. H. Heyne, D. Marinov, N. Braithwaite, A. Goodyear, J.-F. de Marneffe, M. Cooke, I. Radu, E. C. Neyts, and S. D. Gendt, *2D Mater.* **6**, 035030 (2019).
- S. Banna, A. Agarwal, G. Cunge, M. Darnon, E. Pargon, and O. Joubert, *J. Vac. Sci. Technol. A* **30**, 040801 (2012).
- S. Tan, W. Yang, K. J. Kanarik, T. Lill, V. Vahedi, J. Marks, and R. A. Gottscho, *ECS J. Solid State Sci. Technol.* **4**, N5010 (2015).
- J. Robertson, *Rep. Prog. Phys.* **69**, 327 (2005).
- N. Gulbrandsen, Å. Fredriksen, J. Carr, and E. Scime, *Phys. Plasmas* **22**, 033505 (2015).
- R. M. Martin, H.-O. Blom, and J. P. Chang, *J. Vac. Sci. Technol. A* **27**, 217 (2009).
- R. M. Martin and J. P. Chang, *J. Vac. Sci. Technol. A* **27**, 209 (2009).
- C. Steinbrüchel, *Appl. Phys. Lett.* **55**, 1960 (1989).
- P. M. Gevers, H. C. W. Beijerinck, M. C. M. van de Sanden, and W. M. M. Kessels, *J. Appl. Phys.* **103**, 083304 (2008).
- E. Sungauer, E. Pargon, X. Mellhaoui, R. Ramos, G. Cunge, L. Vallier, O. Joubert, and T. Lill, *J. Vac. Sci. Technol. B* **25**, 1640 (2007).
- K. Nakamura, D. Hamada, Y. Ueda, K. Eriguchi, and K. Ono, *Appl. Phys. Express* **2**, 016503 (2009).
- K. J. Kanarik *et al.*, *J. Vac. Sci. Technol. A* **35**, 05C302 (2017).
- E. Sungauer, X. Mellhaoui, E. Pargon, and O. Joubert, *Microelectron. Eng.* **86**, 965 (2009).
- T. Lin *et al.*, *ACS Appl. Mater. Interfaces* **7**, 15892 (2015).